Journal of
Synchrotron Radiation

ISSN 0909-0495

Received 25 October 2011
Accepted 5 March 2012

The SAMBA quick-EXAFS monochromator: XAS with edge jumping

E. Fonda,[a]* A. Rochet,[a,b] M. Ribbens,[a] L. Barthe,[a] S. Belin[a] and V. Briois[a]

[a]Synchrotron SOLEIL, L'Orme des Merisiers, BP 48, Saint Aubin, 91192 Gif sur Yvette, France, and [b]IFP Energies Nouvelles, Etablissement de Lyon, Rond-point de l'échangeur de Solaize, BP 3, 69360 Solaize, France. E-mail: fonda@synchrotron-soleil.fr

Results and performances of the QEXAFS double monochromator of the SAMBA beamline (Synchrotron SOLEIL) are presented. The device is capable of speeds of up to 40 Hz, while giving the user the possibility to choose the amplitude of the scan from 0.1° to 4° in a few seconds. The device is composed of two independent units and it is possible to perform scans alternating between two different crystals, literally jumping from low (4 keV) to high (37 keV) energies.

Keywords: XAS; quick EXAFS; X-ray monochromator; X-ray optics; catalysis; time-resolved spectroscopy.

1. Introduction

Extended X-ray absorption spectroscopy (EXAFS) has more than 60 years of history and, despite the disadvantage of requiring a synchrotron light source for its practical usage, it is a well established and widespread technique employed in different fields such as surface science (Ohta, 1998), life sciences (Strange & Feiters, 2008) and materials science (Gurman, 1982). On one hand, this technique, which provides powerful element-specific atomic-level chemical and geometric information, is very effective for establishing structure–property relationships in any kind of materials. On the other hand, with the advent of bright synchrotron radiation sources and the resulting potential reduction in data collection time, huge opportunities for *in situ* time-resolved EXAFS investigations have emerged in the field of the operando characterization of batteries (Tanida *et al.*, 2011; McBreen *et al.*, 1988) and catalysts (Evans & Tromp, 2010; Ressler *et al.*, 2002; Clausen, 1998), to cite a few.

Quick-EXAFS (QEXAFS) stands for all EXAFS experiments where the X-ray monochromator is mechanically moved continuously and data are collected on the fly (Frahm, 1989; Prieto *et al.*, 1992). This definition encompasses a very broad range of time scales and many authors talk about QEXAFS for time frames spanning from one or more minutes (Clausen *et al.*, 1993; Lee *et al.*, 1998; Bras *et al.*, 2010) to seconds (Frahm, 1988; Als-Nielsen *et al.*, 1995; Proux, 2005) or several milliseconds (Bornebusch *et al.*, 1999; Frahm *et al.*, 2005; Narayanan *et al.*, 2007; Briois *et al.*, 2011). The mechanical movement intrinsic to the QEXAFS technique will set a limit for the speed, while the trend toward faster data acquisition rates is not limited by the spectroscopy itself: energy-dispersive EXAFS, where the optic is static, can be at least as fast as a few milliseconds (Newton *et al.*, 2005) but with severe limitations (Newton *et al.*, 2002; Newton, 2007); finally, pump–probe experiments with synchrotron sources in the slicing mode are able to reach unprecedented time resolutions down to 100 fs (Bressler *et al.*, 2009; Bauer & Bertagnolli, 2009).

Almost all EXAFS beamlines built during the last few years are capable of some form of QEXAFS and of scanning an XANES spectrum (typically 200–300 eV) on the scale of a couple of minutes, since this does not require a dedicated monochromator design (Dent *et al.*, 2009). To perform faster measurements, specific designs are necessary such as the in-vacuum cam-driven design proposed by Frahm and co-workers (Lützenkirchen-Hecht *et al.*, 2005; Stötzel *et al.*, 2008, 2010). This device is installed at the Swiss Light Source (Super-XAS) (Frahm *et al.*, 2010) and seems to be tailored for most QEXAFS experiments covering the range between 25 ms and 1 s. The monochromator mechanism consists of a channel-cut crystal mounted on a tilt table alternatively pushed and pulled by a cam rotating at constant speed. This oscillatory movement covers only the energy range of a scan (typically from one tenth to a few degrees). The system is very simple to align and capable of covering very broad energy ranges by simply choosing a suitable cam amplitude.

The original in-vacuum cam-driven monochromator design has been reworked by our group in SOLEIL to produce the double-QEXAFS monochromator of the SAMBA beamline (Briois *et al.*, 2011). This device was installed and opened to users in 2009 (Renaud *et al.*, 2009).

This paper is devoted to the technical description of the SAMBA Quick-EXAFS monochromator and its performances after almost three years of operation.

2. Experimental

2.1. QEXAFS monochromator description

To perform QEXAFS it is necessary to quickly change the Bragg angle of the monochromator crystal between two values corresponding to the extremes of the desired absorption spectrum and repeat this movement over and over. The solution adopted herein consists of separating the Bragg movement into two parts: one goniometer is used to move the Bragg angle over a large range and another one is used to move faster over a small amplitude (Frahm *et al.*, 2005). The monochromator is modular: a channel-cut crystal is mounted on a first stage that is capable of fast oscillations with an adjustable amplitude and that carries the water-cooling pipes and the heat exchanger. This part is then mounted on a larger goniometer that moves the crystal to the desired Bragg angle. Finally, the goniometer is mounted on a Z stage to align the crystal and keep it on the X-ray beam when the Bragg angle is changed over a large interval (Fig. 1).

The working principle of the fast oscillating stage is illustrated in Fig. 2. Two flexure hinges define the crystal rotation axis (R1 in Fig. 2), and two other flexure hinges (R3 in Fig. 2) connect the crystal to the cam. While the cam rotates around its own axis, it pushes and pulls the crystal stage and the crystal rotates about the R1 axis with an amplitude $\Delta\Theta$. The amplitude of the oscillation of the crystal is defined by the geometry of the links to the cam and by the eccentricity (Δ) of the cam. If the eccentricity is zero, the axis of rotation of the cam would be its own center and no movement will be transmitted to the crystal. An exploded view of the actual cam mechanism is shown in Fig. 3. Changing the eccentricity is accomplished by sliding in or out of the cam the axis R2: the axis has a slit on one side (S in Fig. 3); this slit is diagonal and extends from the center to one corner of part A. When part A is moved inside part B, part B moves on one side and the eccentricity changes.

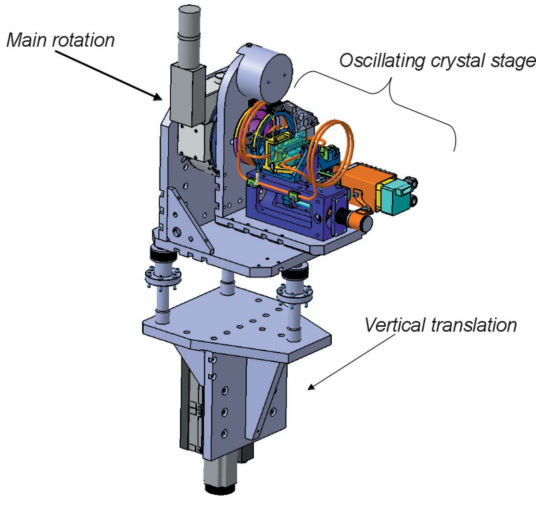

Figure 1
View of the monochromator main components: a vertical motorized stage holds the main rotation; this is necessary to align the oscillating crystal stage to an average Bragg angle. The oscillating stage produces the fast oscillation and controls its amplitude.

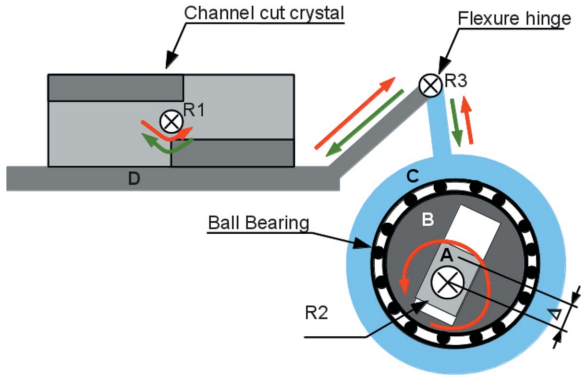

Figure 2
Scheme illustrating the working principle of the variable cam. The crystal rotation axis R1 is defined by two flexure hinges, while the cam rotates around R2. The component A rotates around R2, part B can be moved aside and its center is at distance Δ from R2 defining the eccentricity of the cam. When A rotates, the center of B moves around R2, while part C is connected through a ball-bearing and moves up and down. To transmit the motion of C to the crystal without mechanical play, two other flexure hinges (point R3) are necessary.

A DC servo motor rotates the cam at constant speed and produces the oscillatory movement. A stepper motor moves the cam at the desired eccentricity, while the main goniometer is moved to the desired average Bragg angle by another stepper motor. All movements are encoded; in particular one encoder measures changes in the Bragg angle produced by movements of both the main goniometer and the oscillating stage.

The variable cam has been designed to cover a range from 0.1 to 4° and the amplitude of its movement can be changed within seconds even while moving. The effort sustained by the cam depends on the chosen frequency and amplitude; *e.g.* 40 Hz is the maximum speed if $\Delta\Theta = 1°$, while 10 Hz is the maximum speed if $\Delta\Theta = 4°$. The mechanical limit in oscillation

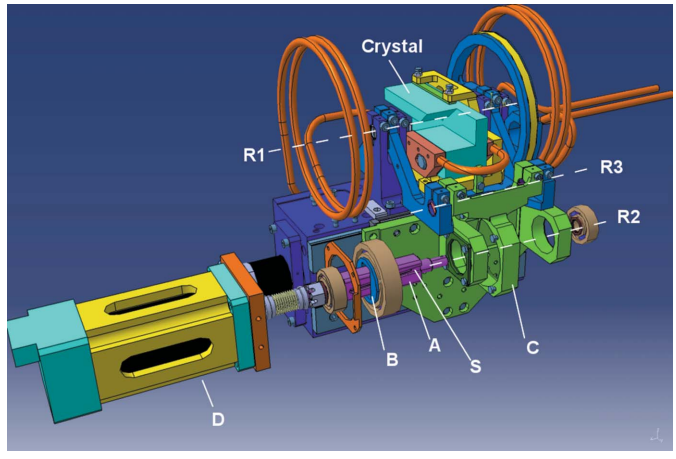

Figure 3
Exploded view of the variable cam mechanism. The crystal (light cyan) rotates around axis R1, while the cam axis is R2. R3 is a moving axis defined by two flexure hinges and connects the cam to the oscillating table. Part A (pink) is the axis of the cam; the slit (S) on its front side is used to attach it to part B (blue). Part B moves up when part A moves towards the left of the picture. The DC motor used to rotate the cam is represented on the left (D).

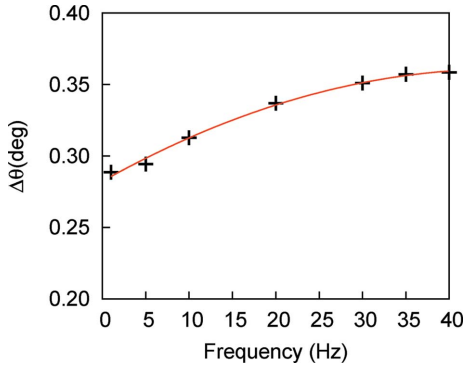

Figure 4
Actual oscillation amplitude as measured by the encoder *versus* the excitation frequency; the nominal amplitude is 0.29°. There is a measurable and fully reversible increase of the amplitude. The curve is not diverging, indicating that the frequency could be further increased.

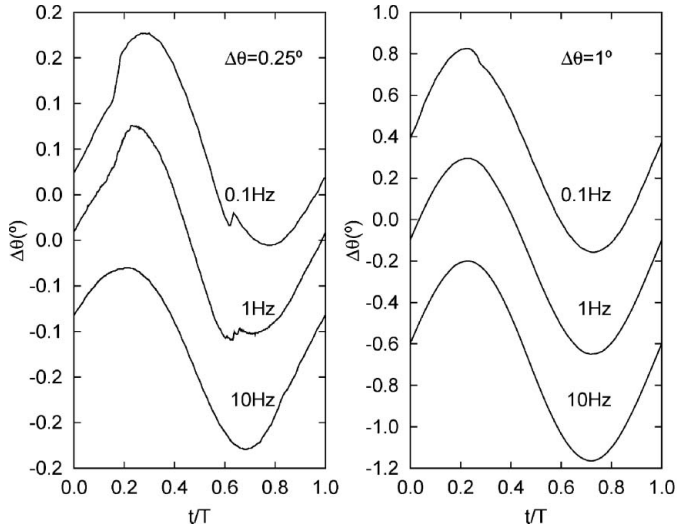

Figure 5
Angular position of the oscillating stage ($\Delta\theta$) as read by the encoder as a function of time. Time is normalized by the oscillation period in order to compare the curves on the same scale. Oscillations of 0.25° and 1° have been recorded at 0.1 Hz, 1 Hz and 10 Hz, increasing speed and amplitude smooth-off irregularities in the movement of the cam as the instantaneous speed increases.

speed is determined first by the servo motor strength and then by the stiffness of the system that determines its resonance frequency. When exciting a system over the resonance frequency, the amplitude of the movement decreases fast with frequency, while below the resonance the amplitude grows for increasing frequency. Tests performed on the monochromator show that the system works well below the resonance, but there is already a measurable amplitude increase with frequency for a given 'nominal' cam amplitude as shown in Fig. 4. The process is fully reversible and reproducible.

The ball-bearing of the cam transmits the motion between parts B and C (compare Figs. 2 and 3); this part is critical since, to allow rotation, it must have a small mechanical play. Another source of play is in the camshaft, that must slide in and out to change the eccentricity.

From our understanding, the play is intrinsic to the present design of the camshaft and it shows up close to direction reversal at slow angular speeds, as illustrated in Fig. 5. As the speed or the angular range is increased, the mechanical play is smoothed out and vanishes: the mechanical play disappears at 1° at a speed of 1 Hz, while, for a small oscillation of 0.25°, mechanical play is no longer visible at 10 Hz, and, at 1 Hz, ripples and irregularities are still present. It is noteworthy that anomalies close to the point of direction reversal should only affect the end or beginning of the spectra and do not hinder the use of the monochromator at low speed. Furthermore, as the encoder follows all anomalies and vibrations, and as we never observed a drift in the encoder position even over 12 h of consecutive scans, the presence of these anomalies is not prejudicial at all to the quality of recorded data. Indeed, we find that it is possible to obtain an accurate spectrum even in the worst cases: XANES spectra of the Au L_3-edge measured at 1 Hz with an oscillation amplitude of 0.25° and 0.8° are indistinguishable (besides noise) from a standard measurement (Fig. 6).

The cam amplitude can be changed even during data acquisition at a speed of 1° s^{-1} (Fig. 7). This is a possibility that is extremely useful for set-up and optimization. As suggested by Stötzel *et al.* (2010), this could be used to measure shorter spectra (XANES) with better statistics during a fast and critical part of a reaction and accumulate longer (EXAFS) spectra during slower parts of a reaction. In Fig. 7 we illustrate the effect of changing the cam amplitude alone, but the user can also adjust the main rotation; this give access to a larger EXAFS range without losing statistics in the pre-edge region. The procedure is transparent to the user, since the same encoder monitors both rotations. The cam speed can also be changed on the fly. All these possibilities can be useful, provided that detector limitations have been taken into account as described by Stötzel *et al.* (2011).

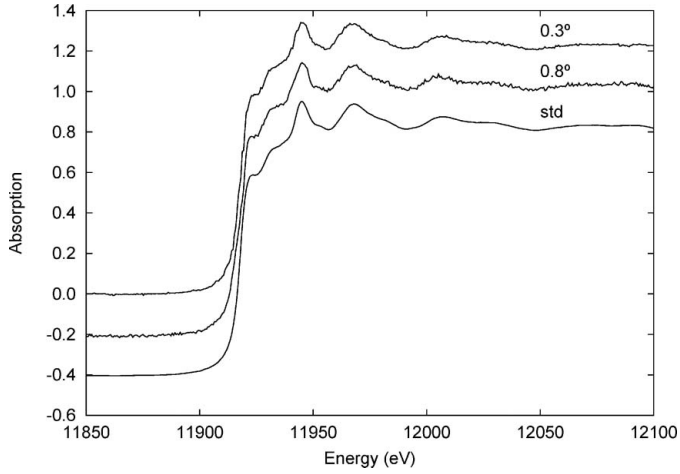

Figure 6
Raw data of Au L_3-edge XANES measured in transmission on a Au metallic foil. Measurements have been made at 1 Hz with an amplitude of 0.25° and 0.8° and compared with a standard measurement (std). Spectra are indistinguishable beside noise. For the spectrum at 0.8° only a part is shown: the noise level on this spectrum is higher since the amplitude of 0.8° is covered in 500 ms and it is compared with a spectrum which is measured over 0.25° in the same time. About 300 s were necessary for the standard spectrum (std).

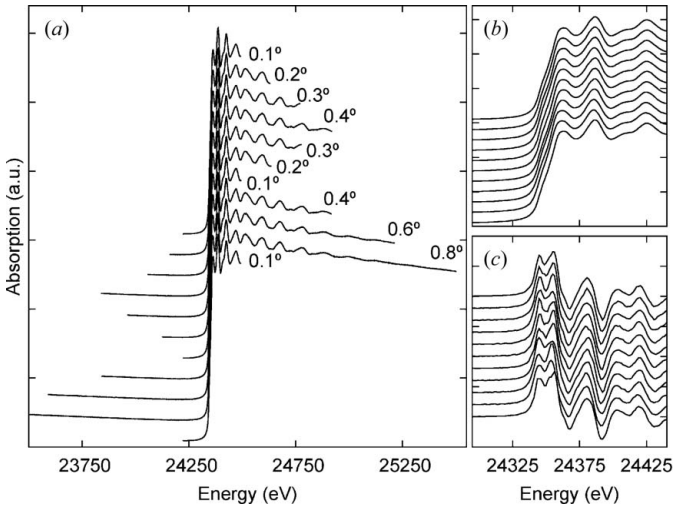

Figure 7
(*a*) Pd *K*-edge XAS measured on a Pd metallic foil; spectra are collected at a rate of 1 Hz. The cam is moved through successive steps to change the oscillation amplitude during the measurement. The time required to change a cam amplitude of 1° is 1 s and the transition from one amplitude to another is virtually invisible (first spectra at the top, last at the bottom). (*b*) Enlarged view of XANES spectra and (*c*) their first derivatives. Spectra have not been realigned or smoothed but simply averaged between successive cam changes to obtain a better signal to noise on the first derivative.

The same vacuum vessel contains two separate monochromators placed one after the other along the beam path (Fig. 8). Each monochromator can move vertically to be aligned on the incoming X-ray beam or to let the beam pass above it. Changing one monochromator for the other can take as long as 20 s. This feature enables us to exchange the monochromators during a slow reaction: Si(311) can be used to access higher energies for diffraction or EXAFS, while Si(111) provides EXAFS at lower energies. This 'edge jumping' (Frahm, 1988, 1991) between really far elements thresholds paves the way for exciting new experiments, as illustrated in §3.1.

We have chosen to build two separate monochromators. Another possibility was to install two crystals facing each other on the same oscillating stage. This option implicitly requires a heavier cradle; this is a very good choice if the device was designed to work from 1 to 10 Hz, while it is a major risk if 40 Hz and more are the target for time resolution, as requested by some experiments in catalysis or electrochemistry.

2.2. Electronics and software for fast data collection

Electronics and software developed to operate data acquisition with the QEXAFS monochromator follow the 'continuous scan' scheme of Synchrotron SOLEIL described by Renaud *et al.* (2009). The angular encoder is read by a scaler card (National Instruments PXI 6602). Ionization chamber currents are amplified by Femto Gmbh DLPCA 200 current-to-voltage amplifiers and the output voltages are digitized by a four-channel 16-bit analog-to-digital converter (ADC, model 2005 by AdLink). Each channel is simultaneously digitized and stored in a separate data buffer. Scaler and ADC are triggered at a user-selectable frequency which is provided by the scaler itself. All elements are configured and controlled through the *TANGO* control system (Götz *et al.*, 2007). A scheme of the system is represented in Fig. 9.

Several ADC cards or scalers can be chained to increase the number of measured quantities: avalanche photodiodes, fluorescence detectors, other encoders or thermocouples. At the time of the writing, the maximum sampling frequency is 300 kHz. The possibility to finely tune the sampling frequency is useful, since it enables the cancellation of spurious periodic signals from the 20 kHz of certain servo motors or other common modes.

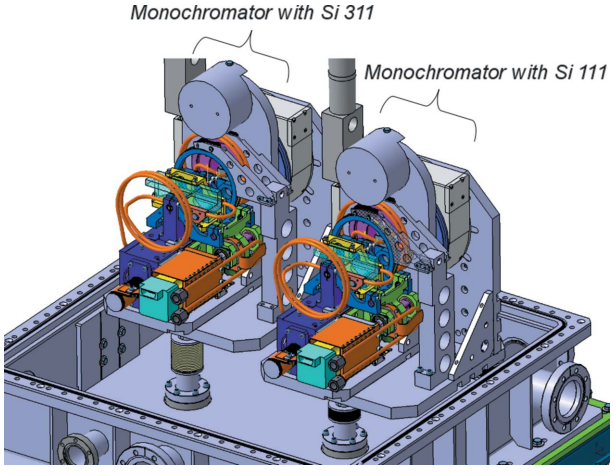

Figure 8
View of the QEXAFS monochromator: two distinct sub-units, each one being an independent QEXAFS monochromator itself, are installed along the X-ray beam path. The unused unit is lowered to allow the beam to pass above the crystal. Only 20 s are necessary to exchange from one monochromator to the other.

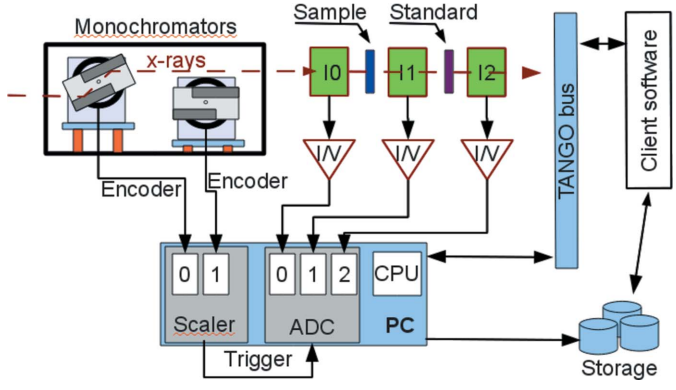

Figure 9
Scheme of the hardware/software system used to acquire data with the QEXAFS monochromator. The scaler card reads the two encoder positions (channels 0 and 1) and provides a trigger at a user-selectable frequency. The storage of encoder values and of analog inputs (ADC channels 0, 1 and 2) is synchronized by this trigger. Double buffering permits the saving of data in the file system while new data are still being recorded. All components are controlled and configured through the *TANGO* software bus.

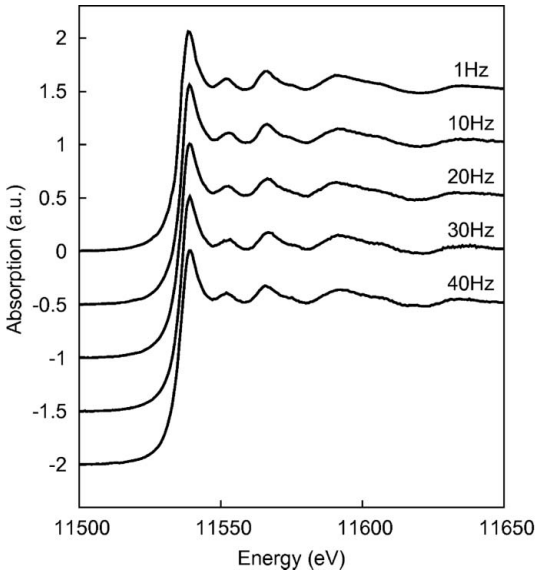

Figure 10
XANES data recorded at the L_3-edge of Pt on metallic Pt foil for different oscillation frequencies over an amplitude of 0.3°; 1 Hz means one spectrum measured in 500 ms, while 40 Hz means one spectrum measured in 12.5 ms. Data are not averaged.

3. Results

Typical XANES spectra are illustrated in Fig. 10, where the L_3-edge of a Pt foil has been measured as a function of the oscillation frequency; the Pt L_3-edge has been chosen for comparison with previous QEXAFS publications (Stötzel *et al.*, 2011) and because of its importance in catalysis. Data quality is good and the XAFS signal is slightly damped only at the maximum oscillation frequency (40 Hz), as expected from the limited ion mobility in ionization chambers.

A major advantage of the SAMBA QEXAFS set-up is its capability to record spectra over a range of 4°. This ensures the collection of an extended EXAFS spectrum (over about 1000 eV), even at the lowest working energy of the beamline, *i.e.* at the Ti *K*-edge (Sauvage-Simkin, 2011). This wide Bragg angle amplitude also allows us to record multiple absorption edges at once (Fig. 11).

3.1. Edge jumping and bimetallic catalysts

A unique feature of the SAMBA QEXAFS is its ability to move from one edge to another even when two different monochromators are needed. The high degree of automation of the beamline permits adjustment of the amplifier gains and the gaseous content of the ionization chambers while changing the monochromator conditions. An example is given by the time-resolved study of the activation of a hydrodesulfurization (HDS) catalyst.

The HDS reaction consists of the catalytic removal of the sulfur heteroelement from gasoline in response to environmental legislations. Industrial HDS catalysts consist of molybdenum sulfide slabs promoted by nickel (or cobalt) and supported on alumina (Song, 2003). Before the activation step, catalysts are composed of metallic oxides; then the active phases are obtained by a sulfidation process in the presence of

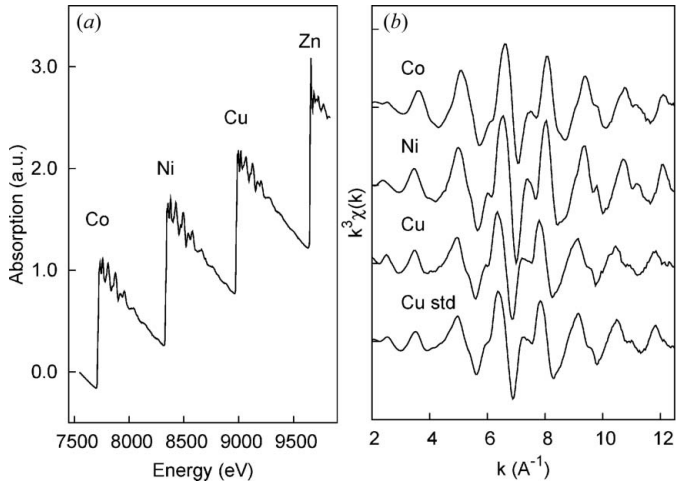

Figure 11
Absorption of a stack of metallic foils: Co, Ni, Cu and Zn, measured in 10 s at a frequency of 1 Hz over an amplitude of 3.6°. XAS (*a*) and EXAFS (*b*) data are shown; a standard measurement on a single Cu foil (Cu std) is shown for comparison.

H_2S. This process, extremely complex at the molecular scale, has a major impact on the activity and the stability of the active phases during the HDS process.

The bimetallic catalyst used in this work consists of 6 wt% Mo and 2 wt% Ni on alumina. The catalyst is mixed with diamond powder and loaded in a dedicated *in situ* cell (Rochet *et al.*, 2011). During XAS analysis, the reactor temperature was increased from room temperature to 673 K at a rate of 2 K min^{-1} with a flow of H_2S/H_2 (15%) at atmospheric pressure [volume of gaseous reactant per volume catalyst per hour (VVH) = 28 min^{-1}]. Using the edge jumping capability, nickel and molybdenum *K*-edges were characterized together on a single sample in a unique experiment. Si(111) and Si(311) crystals were alternatively used for Ni and Mo *K*-edges, respectively. The crystals oscillation frequency was set to 1 Hz providing one spectrum every 500 ms. The dead-time between the start of recording at the Ni *K*-edge and at the Mo *K*-edge was optimized to 60 s; switching monochromators took less time than changing gases in the ionization chambers between Ar and N_2. Gas composition is not stable at the beginning of each measurement; nonetheless, filling chambers simultaneously and having very similar gas contents in all of them was much more important than waiting for stabilization. EXAFS data[1] are stable during the observation time, while the current in the ionization chambers can slowly drift as the gas content stabilizes.

As every edge was measured for 60 s and the monochromator change took 60 s, the temperature difference between a Ni and Mo successive measurement is 4 K (heating at 2 K min^{-1}).

We simultaneously observed the sulfidation of nickel and molybdenum forming the active phase (Fig. 12). To estimate

[1] Supplementary data for this paper are available from the IUCr electronic archives (Reference: IE5068). Services for accessing these data are described at the back of the journal.

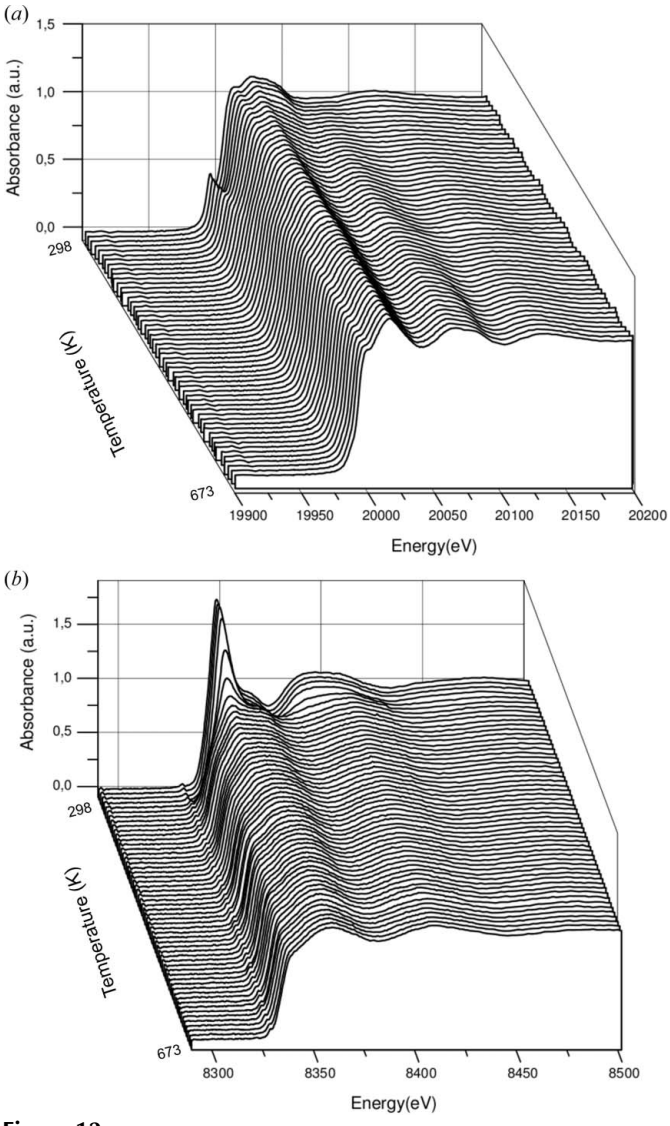

Figure 12
XANES spectra obtained during the activation under H_2S/H_2 of the NiMo catalyst as a function of temperature (2 K min^{-1}) of the Mo *K*-edge (*a*) and Ni *K*-edge (*b*); each spectrum is averaged over 60 s and the monochromator is changed every 60 s to measure alternatively the Mo and Ni absorption edges.

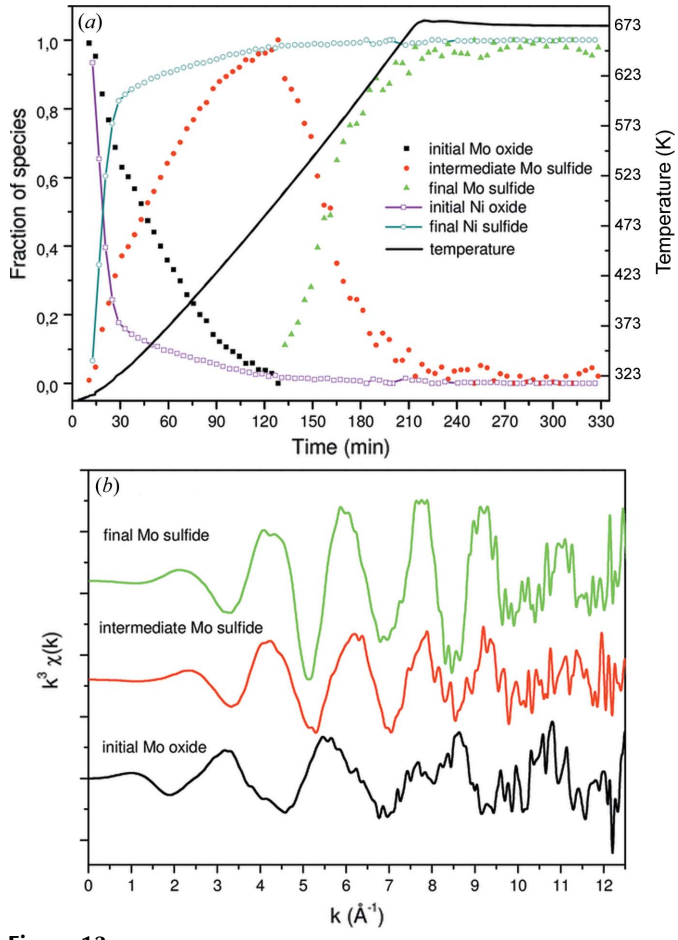

Figure 13
(*a*) Nickel and molybdenum phase compositions during activation under H_2S/H_2 of the NiMo catalyst. (*b*) Mo *K*-edge EXAFS spectra recorded at the beginning, at the maximum of the intermediate Mo sulfide formation and after the formation of the final Mo sulfide. Each spectrum corresponds to an average over 1 min (60 spectra).

the fraction of sulfide species in the catalyst as a function of time, we used a linear combination of the XANES spectrum of the fresh catalyst and of the spectrum collected after sulfidation at 673 K. Actually, only two components were present in the spectra of Ni, while three components were necessary to fit the Mo spectra. An intermediate oxysulfide $\{MoOS_2\}$ phase was revealed to be an intermediate species and it was added for fitting. Adding this component is justified by the presence of two distinct sets of isosbestic points before and after 473 K and by the presence of a maximum in the residual of the fit performed with initial and final components only. Components fractions for Ni and Mo species are plotted *versus* time in Fig. 13.

For the nickel species, the sulfidation started at a low temperature. The sulfidation rate is fast. At 323 K, 80% of Ni is already transformed into the final sulfide phase. At 493 K it is totally sulfided. As far as can be observed by QEXAFS, the structure remains unchanged up to 673 K.

The Mo conversion rate was slower and we distinguished three regions in the sulfidation mechanism. The first region defines the temperature range in which molybdenum is present in the oxidic form. In the second region (around 473 K) the oxysulfide intermediate species is observed. In a third stage, the oxysulfide molybdenum species is transformed into the final product MoS_2. MoS_2 started to appear when Ni was already totally sulfided.

It is generally considered that the sulfidation of Mo occurring simultaneously or before the sulfidation of Ni leads to the formation of the mixed NiMoS active phase (Kubota *et al.*, 2010). In our case Ni is sulfided before Mo, favoring the formation of catalytic inactive Ni sulfided species.

'Edge jumping' provided unique knowledge of the order of occurrence of sulfidation processes for both metallic species. Moreover, this capability is useful for diffraction/absorption studies: we were able to acquire EXAFS spectra on Fischer–Tropsch cobalt-supported catalysts at the Co edge with Si(111), while Si(311) was used to acquire diffraction images at a fixed energy around the Mo *K*-edge (Rochet, 2011).

3.2. Fluorescence yield spectra for diluted specimens

One of the historical advantages claimed for QEXAFS over energy-dispersive EXAFS is the possibility of fluorescence or electron yield measurements; fluorescence yield measurements are by far the best adapted to studies concerning chemistry (solutions, cells) where windows usually confine the sample in a complex atmosphere. While ionization chambers are detectors limited at very high photon fluxes, energy-dispersive detectors commonly used for EXAFS measurements are unusable at frequencies above 0.1 Hz, since they are limited to about 100 kcounts s^{-1}. This limitation is given by solid-state detector electronics or, in the case of monochromator-based detectors, by photon statistics. We find a good compromise in the use of Si avalanche photodiodes (APDs) that can handle up to 10 Mcounts s^{-1} and are so small that they can be put very close to the sample, increasing the collection angle. The disadvantage is the lack of energy resolution. Energy resolution can only be partially recovered using appropriate absorbing filters, thus sensitivity is penalized for very diluted species as described by Warburton (1986). Two other types of detectors can be used: scintillators with a photomultiplier tube connected in current mode or an ionization chamber (Stern *et al.*, 1982).

Fig. 14 shows a spectrum taken on a copper chloride solution in water (10^{-2} *M*). Acquisition took 10 s over a 100 mm^2 APD supplied by Oxford Danfysik, the signal-to-noise ratio is about 110 and the incoming X-ray flux was about 10^{10} photons s^{-1}. The combination of Soller slits, filters and more photons per second on the sample will improve the signal-to-noise ratio which is not yet limited by the APD performance.

4. Conclusions

The design and performance of the SAMBA QEXAFS monochromator have been described, including its edge jumping capability. Since photon statistics are the main limiting factor for QEXAFS on SAMBA, a new beamline has been financed in 2011 by the Agence Nationale pour la Recherche through an EQUIPEX funding. The starting ROCK project concerns a new Synchrotron SOLEIL beamline fully dedicated to QEXAFS. The new beamline will be designed to specifically fit the needs of catalysis and electrochemistry studies. ROCK should open before the end of 2014, while the SAMBA beamline will continue its operations without this QEXAFS monochromator.

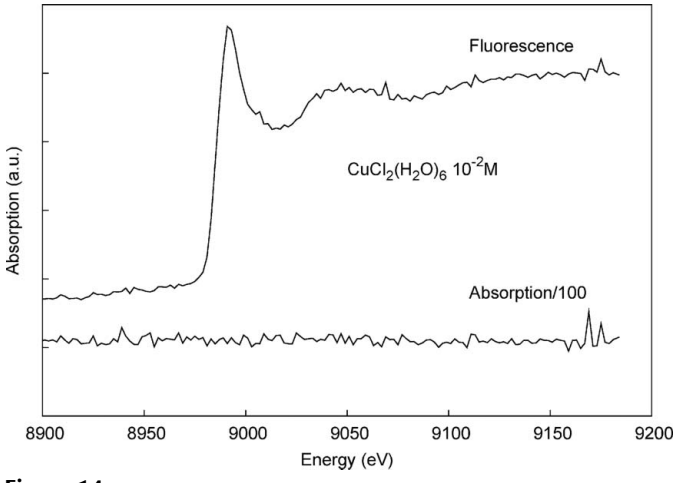

Figure 14
Fluorescence and absorption spectra obtained on an aqueous solution of $CuCl_2(H_2O)_6$ (10^{-2} *M*). Data have been collected in 10 s using a silicon avalanche photodiode. The absorption spectrum is divided by 100 to reduce noise and to fit in the figure. Spectra have been collected simultaneously.

The authors would like to thank B. Baubet from IFP Energies Nouvelles for the synthesis of catalysts. F. Langlois, G. Renaud and A. Noureddine of Synchrotron SOLEIL are acknowledged for their continuous support and for the development of the dedicated electronics and informatics. We would like to thank M. Bordessoule of Synchrotron SOLEIL for the helpful discussions on detectors.

References

Als-Nielsen, J., Grübel, G. & Clausen, B. S. (1995). *Nucl. Instrum. Methods Phys. Res. B*, **97**, 522–525.
Bauer, M. & Bertagnolli, H. (2009). *Chem. Phys. Chem.* **10**, 2197–2200.
Bornebusch, H., Clausen, B. S., Steffensen, G., Lützenkirchen-Hecht, D. & Frahm, R. (1999). *J. Synchrotron Rad.* **6**, 209–211.
Bras, W., Nikitenko, S., Portale, G., Beale, A., van der Eerden, A. & Detollenaere, D. (2010). *J. Phys. Conf. Ser.* **247**, 012047.
Bressler, Ch., Milne, C., Pham, V. T., Elnahhas, A., van der Veen, R. M., Gawelda, W., Johnson, S., Beaud, P., Grolimund, D., Kaiser, M., Borca, C. N., Ingold, G., Abela, R. & Chergui, M. (2009). *Science*, **323**, 489–492.
Briois, V., Fonda, E., Belin, S., Barthe, L., La Fontaine, C., Langlois, F., Ribbens, M. & Villain, F. (2011). *UVX 2010-10e Colloque sur les Sources Cohérentes et Incohérentes UV, VUV et X; Applications et Développements Récents*, pp. 41–47 (http://dx.doi.org/10.1051/uvx/2011006).
Clausen, B. S. (1998). *Catal. Today*, **39**, 293–300.
Clausen, B. S., Gråbaek, L., Steffensen, G., Hansen, P. L. & Topsøe, H. (1993). *Catal. Lett.* **20**, 23–36.
Dent, A. J., Cibin, G., Ramos, S., Smith, A. D., Scott, S. M., Varandas, L., Pearson, M. R., Krumpa, N. A., Jones, C. P. & Robbins, P. E. (2009). *J. Phys. Conf. Ser.* **190**, 012039.
Evans, J. & Tromp, M. (2010). *Heterogenized Homogeneous Catalysts for Fine Chemicals Production*, edited by P. Barbaro and F. Liguori, pp. 433–448. Berlin: Springer.
Frahm, R. (1988). *Nucl. Instrum. Methods Phys. Res. A*, **270**, 578–581.
Frahm, R. (1989). *Rev. Sci. Instrum.* **60**, 2515–2518.
Frahm, R. (1991). *X-ray Absorption Fine Structure*, edited by S. S. Hasnain, pp. 731–737. Chichester: Ellis Horwood.
Frahm, R., Nachtegaal, M., Stotzel, J., Harfouche, M., van Bokhoven, J. A. & Grunwaldt, J.-D. (2010). *AIP Conf. Proc.* **1234**, 251–255.
Frahm, R., Richwin, M. & Lützenkirchen-Hecht, D. (2005). *Phys. Scr.* T**115**, 974.
Götz, A., Meyer, J., Taurel, E., Chaize, J. M., Verdier, P., Poncet, F., Ounsy, F. M., Leclercq, N., Buteau, A. & Scafuri, C. (2007). *Proceedings of International Conference on Accelerator and Large Experimental Physics Control Systems 2007 (ICALEPCS07)*, Knoxville, Tennessee, USA (http://epaper.kek.jp/ica07/PAPERS/FOPA01.PDF).
Gurman, S. J. (1982). *J. Mater. Sci.* **17**, 1541–1570.

Kubota, T., Rinaldi, N., Okumura, K., Honma, T., Hirayama, S. & Okamoto, Y. (2010). *Appl. Catal. A*, **373**, 214–221.
Lee, J. M., Sung, N.-E., Park, J.-K., Yoon, J.-G., Kim, J.-H., Choi, M.-H. & Lee, K.-B. (1998). *J. Synchrotron Rad.* **5**, 524–526.
Lützenkirchen-Hecht, D., Grunwaldt, J. D., Richwin, M., Griesebock, B., Baiker, A. & Frahm, R. (2005). *Phys. Scr.* T**115**, 831.
McBreen, J., O'Grady, W. E. & Pandya, K. I. (1988). *J. Power Sources*, **22**, 323–340.
Narayanan, S., Sandy, A. R., Sprung, M., Sullivan, J., Preissner, C. & Shu, D. (2007). *AIP Conf. Proc.* **879**, 911–914.
Newton, M. A. (2007). *J. Synchrotron Rad.* **14**, 372–381.
Newton, M. A., Dent, A. J. & Evans, J. (2002). *Chem. Soc. Rev.* **31**, 83–95.
Newton, M. A., Fiddy, S. G., Guilera, G., Jyoti, B. & Evans, J. (2005). *Chem. Commun.* pp. 118–120.
Ohta, T. (1998). *J. Electron Spectrosc. Relat. Phenom.* **92**, 131–137.
Prieto, C., Lagarde, P., Dexpert, H., Briois, V., Villain, F. & Verdaguer, M. (1992). *Meas. Sci. Technol.* **3**, 325–329.
Proux, O., *et al.* (2005). *Phys. Scr.* T**115**, 970.
Renaud, G., Abeille, G., Elkaim, E., Fonda, E., Langlois, F. & Malik, J. (2009). *Proceedings of the International Conference on Accelerators and Large Experimental Physics Control Systems 2009 (ICALEPCS2009)*, Kobe, Japan (http://epaper.kek.jp/icalepcs2009/papers/wep054.pdf).
Ressler, T., Wienold, J., Jentoft, R. E., Neisius, T. & Günter, M. M. (2002). *Top. Catal.* **18**, 45–52.
Rochet, A. (2011). PhD thesis, Paris-Sud, France.
Rochet, A., Moizan, V., Pichon, C., Diehl, F., Berliet, A. & Briois, V. (2011). *Catal. Today*, **171**, 186–191.
Sauvage-Simkin, M. (2011). *L'Actualité Chimique*, October–November 2011, No. 356–357.
Song, C. S. (2003). *Catal. Today*, **86**, 211–263.
Stern, E. A., Elam, W. T., Bunker, B. A., Lu, K. & Heald, S. M. (1982). *Nucl. Instrum. Methods*, **195**, 345–346.
Stötzel, J., Lützenkirchen-Hecht, D., Fonda, E., De Oliveira, N., Briois, V. & Frahm, R. (2008). *Rev. Sci. Instrum.* **79**, 083107.
Stötzel, J., Lützenkirchen-Hecht, D. & Frahm, R. (2010). *Rev. Sci. Instrum.* **81**, 073109.
Stötzel, J., Lützenkirchen-Hecht, D. & Frahm, R. (2011). *J. Synchrotron Rad.* **18**, 165–175.
Strange, R. W. & Feiters, M. C. (2008). *Curr. Opin. Struct. Biol.* **18**, 609–616.
Tanida, H., Yamashige, H., Orikasa, Y., Oishi, M., Takanashi, Y., Fujimoto, T., Sato, K., Takamatsu, D., Murayama, H., Arai, H., Matsubara, E., Uchimoto, Y. & Ogumi, Z. (2011). *J. Synchrotron Rad.* **18**, 919–922.
Warburton, W. K. (1986). *Nucl. Instrum. Methods Phys. Res. A*, **246**, 541–544.